Journal of Solid State Chemistry 181 (2008) 2620–2625

Contents lists available at ScienceDirect

Journal of Solid State Chemistry

journal homepage: www.elsevier.com/locate/jssc

Controllable preparation and properties of composite materials based on ceria nanoparticles and carbon nanotubes

Changqing Li, Nijuan Sun, Jiangfeng Ni, Jinyong Wang, Haibin Chu, Henghui Zhou, Meixian Li, Yan Li *

Beijing National Laboratory for Molecular Sciences, National Laboratory of Rare Earth Material Chemistry and Application, Key Laboratory for the Physics and Chemistry of Nanodevices, College of Chemistry and Molecular Engineering, Peking University, Beijing 100871, China

ARTICLE INFO

Article history:
Received 1 April 2008
Received in revised form
16 June 2008
Accepted 19 June 2008
Available online 24 June 2008

Keywords:
Carbon nanotube
Ceria
Composite
Electrochemical property
Nanocrystal

ABSTRACT

We report a method to prepare composites based on carbon nanotubes (CNTs) and CeO_2 nanoparticles (NPs). The CeO_2 NPs were attached to CNTs by hydrothermal treatment of $Ce(OH)_4$/CNT mixture in NaOH solution at 180 °C. It was found that larger CeO_2 NPs were formed in the presence of CNTs. Grain size of CeO_2 NPs in the composites can be reduced when $NaNO_3$ was added in the hydrothermal process. Electrochemical characterizations have shown that the composites possess a specific capacity between those of CNTs and CNTs mechanically mixed with CeO_2. These CeO_2/CNT composites could serve as promising anode materials for Li-ion batteries.

1. Introduction

Nanocomposites of carbon nanotubes (CNTs) and inorganic nanoparticles (NPs) have attracted much attention owing to their unique properties and a wide range of applications in catalysis [1,2], sensing [3,4], and energy storage [5–7]. In the composite, CNTs can serve as high-performance support because of their large surface area, exceptional electrical properties, unusual mechanical stability, and unique hollow tubular herringbone structures. NPs can be uniformly dispersed on the sidewalls of CNTs and have electronic charge transfer with CNTs in either covalent or noncovalent interactions [8,9]. As a result, the composites of NPs and CNTs can provide NP-based materials with significantly improved performance.

Because of its unique redox properties, high oxygen storage capacity, and strong ultraviolet absorption, CeO_2 has been extensively applied in catalysis [10], solid oxide fuel cells [11] and optics [12]. For instance, CeO_2 is an indispensable component in three-way catalysts to reduce air pollution in automobile exhaust. The formation of oxygen vacancies, which reduces Ce^{4+} to Ce^{3+}, plays a critical role in the catalytic reactions. Recently, it was found that the reduction capability of the oxygen vacancies was enhanced in CeO_2 NPs [13], providing a very promising route to produce high-activity catalyst.

To incorporate the unique properties of CNT and CeO_2, many efforts have been made to prepare composite materials of CNTs and CeO_2 NPs, including precipitation in solution [14–17], hydrothermal process [18], and ultrasonic preparation [19]. For example, Wei et al. [15] deposited $Ce(OH)_3$ precipitate on CNTs and then heated the product at 450 °C in air to obtain CeO_2/CNT composites. Although the aggressive thermal oxidation can efficiently convert $Ce(OH)_3$ to CeO_2, CNTs could be damaged and even completely destroyed [14]. Relatively mild hydrothermal route [18] is more advantageous, because it can prepare NPs with high-degree crystallinity, homogeneous composition and controllable morphology while avoiding the damage to CNTs. However, the reported hydrothermal treatment temperature is still high (up to 390 °C), therefore limits its application [18]. In the present study, we report the hydrothermal treatment of $Ce(OH)_4$/CNT precursor at a relatively low temperature (180 °C) to prepare CeO_2/CNT composites. We show that composites of crystalline NPs and undamaged CNTs can be synthesized and the morphology of NPs can be adjusted by controlling hydrothermal treatment conditions. We examined the composites with electrochemical charge/discharge cycle to explore their usage as battery materials.

2. Experimental

2.1. Synthesis

CNTs with diameters of 10–20 nm were purchased from Shenzhen Nanotech Port Co. Ltd., China. The CNTs were oxidized by refluxing at 130 °C in concentrated nitric acid for 12 h to introduce carboxyl and hydroxyl groups on the ends and sidewalls

* Corresponding author. Fax: +86 10 62756773.
E-mail address: yanli@pku.edu.cn (Y. Li).

0022-4596/$ - see front matter © 2008 Elsevier Inc. All rights reserved.
doi:10.1016/j.jssc.2008.06.040

of CNTs [20]. All the other starting materials were analytical grade and used as purchased.

The CeO_2/CNT composites were prepared by hydrothermal treatment of the mixture of ceria precursors and CNTs. $CeCl_3$ and $(NH_4)_2Ce(NO_3)_6$ were used as the ceria precursors, respectively. In experiments with $CeCl_3$ as the precursor, 10 mg of oxidized CNTs dispersed in 20 mL deionized water was mixed with 15 mL 0.02 M $CeCl_3$ solution. After the mixture was sonicated for 20 min, 1%(w/w) NaOH was used to titrate pH to ~10 under constant magnetic stirring. The slurry product was stirred for two more hours and then exposed for over 20 h to oxidize the $Ce(OH)_3$/CNT to $Ce(OH)_4$/CNT thoroughly.

With $(NH_4)_2Ce(NO_3)_6$ as the ceria precursor, $Ce(OH)_4$ was precipitated on the sidewalls of CNTs in a short time. The mixture was separated by centrifugation. The $Ce(OH)_4$/CNT product was then mixed with 10 mL 5 M NaOH solution and transferred into a stainless steel autoclave with a Teflon liner of 20 mL volume. After heated at 180 °C for 45 h, the solution was separated by centrifugation, washed with deionized water for three times, and then dried at 60 °C. For comparison, CeO_2 NPs were also prepared with the same process except for the absence of CNTs.

2.2. Characterization

Transmission electron microscope (TEM, JEOL-200 CX) and high-resolution transmission electron microscope (HRTEM, Tecnai F30) were used to determine the size and morphology of the CeO_2/CNT composites. In total, 100 CeO_2 NPs were measured in TEM images to obtain the average particle size. X-ray diffraction (XRD) measurements were performed on a Rigaku Dmax-2000 X-ray diffractometer with Cu$K\alpha$ radiation ($\lambda = 1.5406$ Å) at an accelerating voltage of 40 kV. Crystallite size of the CeO_2 NPs was calculated from diffraction patterns with the Scherrer equation.

Cyclic voltammetry in 0.1 M H_2SO_4 was used to characterize electrochemical performance of the composites with a CHI 660A electrochemical working station (CH Instrument, Inc.) in a regular three-electrode cell. A glassy carbon (GC) electrode (diameter = 4 mm) was used as the working electrode, a platinum wire was used as the counter electrode, and a KCl-saturated calomel electrode served as the reference electrode. Typically, 5 mg of the composite was dispersed in 5 mL deionized water under sonication for 2 h and 15 μL suspension was cast on the GC electrode. Finally, the GC electrode was dried under an infrared lamp.

The electrochemical charge and discharge tests of the products were performed on a Land battery test system. To prepare the composite electrode, 80% (w/w) composite, 10% (w/w) acetylene black, and 10% (w/w) of polytetrafluoroethylene binder were thoroughly blended in alcohol and then rolled into a 0.2 mm thick sheet. The sheet was then punched into a 7 mm diameter disk. Li metal foil was used as the counter electrode with a Celgard 2400 microporous polypropylene film as the separator. A total of 1 M $LiPF_6$ in ethylene carbonate/diethyl carbonate/ethyl methyl carbon (1:1:1 by volume) solution was used as electrolyte. Finally, the electrodes were assembled into Swagelok cells at 25 °C in a dry room with relative humidity of ~1%.

3. Results and discussion

3.1. CNT-induced size increase of CeO_2 NPS

TEM and HRTEM images of the CeO_2/CNT composites prepared from $Ce(OH)_4$/CNT precursors and CeO_2 NPs from $Ce(OH)_4$ precursors in the hydrothermal processes were shown in Fig. 1a–g, respectively. When $CeCl_3$ was used as the cerium source, CNTs were densely coated with CeO_2 NPs. Clear lattice fringes were observed in HRTEM images, indicating that crystalline particles formed in the hydrothermal process. In contrast, the composites prepared from $(NH_4)_2Ce(NO_3)_6$ as cerium precursor possessed sparely dispersed CeO_2 NPs anchored on the sidewalls of CNTs. The average sizes of the CeO_2 NPs in the CeO_2/CNT composites prepared from $CeCl_3$ and $(NH_4)_2Ce(NO_3)_6$ are 16.2 ± 5.0 and 18.7 ± 4.2 nm, respectively. In the absence of CNTs, the size of CeO_2 NPs is ~7.5 nm. It is clear that the presence of CNTs can significantly increase the size of CeO_2 NPs.

CNT-induced size increase of CeO_2 NPs was also confirmed by the XRD measurement (Fig. 2). The CeO_2/CNT composite and free CeO_2 NPs derived from the hydrothermal treatment had well-defined diffraction peaks ascribed to fluorite-structured CeO_2. Weak and broad peaks corresponding to (111), (200), (220), and (311) crystal facets in fluorite structured CeO_2 (JPCDS 34-0394) were clearly observed from the CeO_2 NPs converted from $Ce(OH)_3$ precipitation with $CeCl_3$ as precursor and with no CNTs. However, relatively sharp peaks were observed from the CeO_2/CNT composites, indicating that the CNT-supported CeO_2 NPs significantly increased grain size and possessed higher degree of crystallinity. Estimated with the Scherrer formula, the average grain size of CeO_2 NPs in the CeO_2/CNT composite was ~16.1 nm. The size was remarkably larger than that of the CeO_2 NPs prepared in the absence of CNTs (~7.1 nm). Similar trend has also observed from the XRD patterns obtained from the samples prepared with $(NH_4)_2Ce(NO_3)_6$ as the cerium source (Figure S1 in Supplementary data).

Wu et al. [21] explained the reason why small-sized CeO_2 NPs could be obtained from the hydrothermal treatment of $Ce(OH)_4$ precursor in basic solution by a dissolution–recrystallization mechanism. However, it is obvious that their explanation could not be applied to explain the larger CeO_2 particles formed in presence of CNTs in our observation. Furthermore, we replaced CNTs with nylon fiber to investigate the influence of heterogeneous nucleation at the same experimental conditions. Nylon polymer contains repeat units of amide linkages, which can also provide the heterogeneous nucleation sites for CeO_2 NPs. However, the size increase of CeO_2 NPs in the composites was not observed (Figure S2 in Supplementary data), which means the influence of heterogeneous nucleation should be excluded.

Here, we attributed the size increase of CeO_2 NPs on CNTs to redox reaction between CNTs and CeO_2 NPs during the hydrothermal process. According to our examination, within 12 h, particles formed from the $Ce(OH)_4$/CNT precursor had similar size as those from the $Ce(OH)_4$ precursor, which was consistent with the results reported in literature [22]. Based on this observation, we concluded that CeO_2 NPs were nucleated in the early stage during the hydrothermal treatment, and then grew larger via a subsequent ripening stage.

It is obvious that negatively charged functional groups such as carboxylic group on the sidewalls of CNTs can absorb positive charged Ce(IV) species, which may act as the nucleation center [23]. Those nuclei could initiate the growth of CeO_2 NPs, which were attached tightly to CNTs. It is known that CeO_2 can both store and release oxygen depending on the redox potential of the adsorbate on its surface through the conversion between Ce^{4+} and Ce^{3+} [24]. It has been reported that soot particles are more likely to be oxidized by the active lattice oxygen atoms in CeO_2 than oxygen in air at 400 °C [25]. For the CeO_2 NPs/CNT composite, in the early stage of hydrothermal treatment, small CeO_2 NPs were formed on the CNT sidewalls, and a large portion of oxygen atoms with higher activity were exposed on the surface. In addition, CNTs are more active than soot because of the π-orbital mismatch caused by an increased curvature of the nanotube surface [26]. Therefore, the oxygen atoms of CeO_2 NPs could interact with the

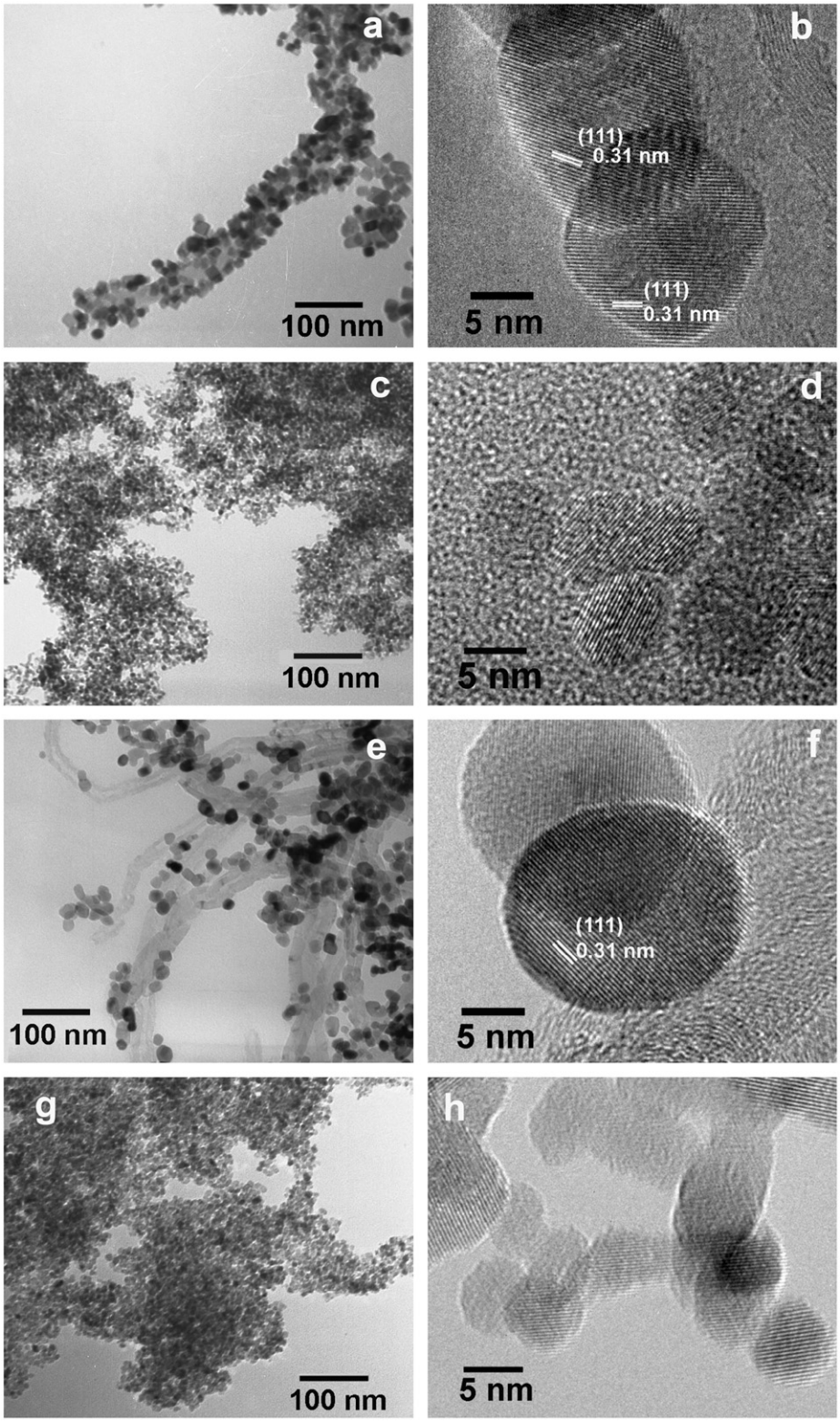

Fig. 1. TEM and HRTEM images of CeO_2/CNT composites and CeO_2 nanoparticles obtained via the hydrothermal treatment of $Ce(OH)_4$/CNT precursors (a, b, e, f) and $Ce(OH)_4$ precipitates (c, d, g, h) in the presence of 5 M NaOH at 180 °C for 45 h with $CeCl_3$ (a–d) and $(NH_4)_2Ce(NO_3)_6$ (e–h) as the cerium source.

curved sp^2-hybridized carbon atoms of CNTs and became weakly bonded. Once the oxygen vacancies are formed, the neighboring Ce^{4+} ion is reduced to Ce^{3+} ion. As the number of Ce^{3+} ions increased in a concentrated basic solution, anisotropic $Ce(OH)_3$ nuclei would be formed and reach a new dissolution–deposition equilibrium. Though the $Ce(OH)_3$ nuclei are unstable and easy to be oxidized to CeO_2 at 180 °C, they could serve as nuclei for larger crystalline CeO_2 particles [22]. We suggest that the formation of $Ce(OH)_3$ nuclei promoted by CNTs eventually lead to the larger CeO_2 NPs in the final stage. To verify our hypothesis, we introduced a number of reducing reagents including hydrazine hydrate, hydroxylamine hydrochloride, 1,4-phthalaldehyde, and

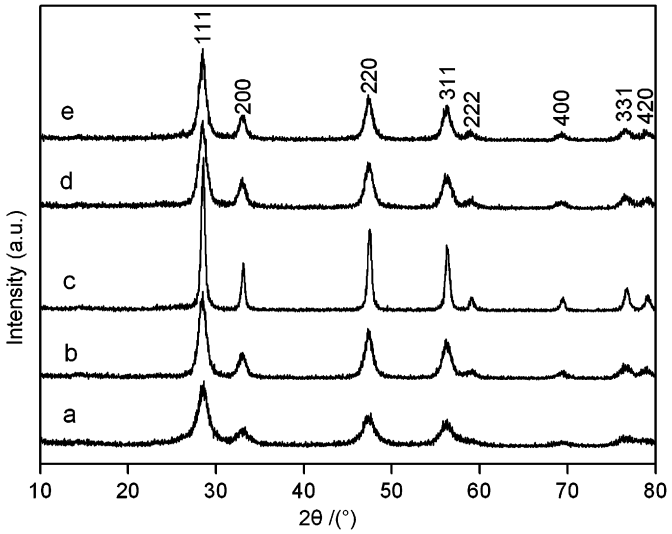

Fig. 2. XRD patterns of $Ce(OH)_4$ precursor dried at 60 °C (a), CeO_2 NPs (b, d) and CeO_2/MWNT composites (c, e) prepared by hydrothermally aging $Ce(OH)_4$ and $Ce(OH)_4$/CNT precursors at 180 °C for 45 h, respectively. (b, c) Without the addition of $NaNO_3$, (d, e) in the presence of $NaNO_3$. $CeCl_3$ was used as the cerium source.

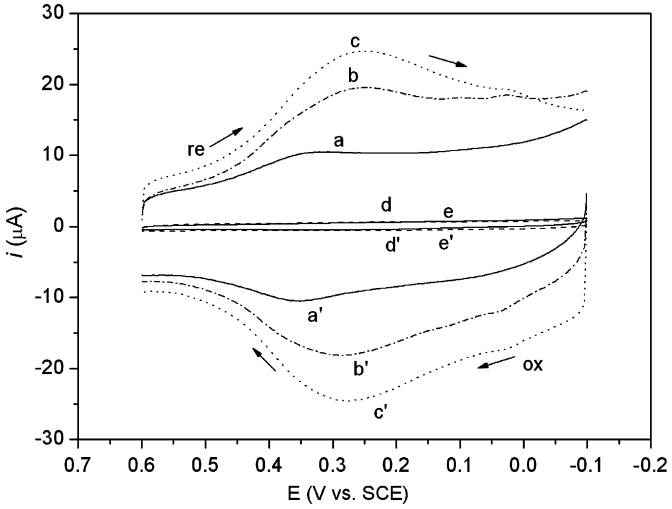

Fig. 3. Cyclic voltammetry (CV) graph of CeO_2/CNT composite(a, a′), the mixture of hydrothermal-treated CeO_2 and oxidized CNTs (b, b′), oxidized CNTs (c, c′), CeO_2 nanoparticles (d, d′), and bare GCE (e, e′).

hydroquinone to react with CeO_2 NPs. As expected, the obtained CeO_2 particles had various degree of increase in diameters (Figure S3 in Supplementary data). Furthermore, with fresh $Ce(OH)_3$ precursors prepared from $CeCl_3$ and NaOH in the same hydrothermal treatment, the resultant CeO_2 NPs were much bigger than those formed with $Ce(OH)_4$ precursors (Figure S4 in Supplementary Data). However, the CeO_2 NPs in CeO_2/CNT were smaller than those just with $Ce(OH)_3$ which might be due to the weaker reducing ability of CNTs and therefore less Ce(III) was formed.

Owing to the oxidation by the active lattice oxygen of CeO_2 NPs, CNTs with the oxygen-containing surface groups could possess different redox potentials. To examine the potential of the composite, we performed cyclic voltammetric (CV) measurements of glass carbon (GC) electrodes functionalized with CNTs, CeO_2 NPs, CeO_2/CNT composite, and CNTs mixed with CeO_2 NPs, respectively, in H_2SO_4 (Fig. 3). Here, CeO_2 NPs and CeO_2/CNT composites were both obtained at hydrothermal conditions using $(NH_4)_2Ce(NO_3)_6$ as the cerium source. For CNTs, the reduction and oxidization peaks associated with the oxygen-containing surface groups were at 0.240 and 0.288 V, respectively. In contrast, the oxidation peak of CNTs in the CeO_2/MWNT composite was shifted to 0.363 V, and the reduction peak to 0.317 V. These shifts were not caused by the redox reactions of CeO_2 NPs for no electrochemical signal of CeO_2 NPs appeared in the corresponding potential range. Additionally, the mechanically mixed CNTs and CeO_2 NPs give the same peak potential as those with pure CNTs. Therefore, the increased oxidation potential of CNTs undoubtedly resulted from the oxidization of CNTs during the hydrothermal process [27]. This result further proves that during the aging process in hydrothermal treatment, CeO_2 can be reduced to Ce(III) species by the CNTs, which will result in the morphological change of the CeO_2 NPs.

3.2. Effects of $NaNO_3$ on the particle size

We introduced commonly used salts including NaCl, Na_2SO_4, CH_3COONa, and $NaNO_3$ into the hydrothermal process to investigate their influences on the morphology of the CeO_2 NPs. Only the addition of $NaNO_3$ remarkably affected the size of CeO_2 NPs. When $CeCl_3$ was used as the cerium source, CeO_2 NPs were closely packed on the CNT surface, and the particle size dramatically decreased with increased concentration of $NaNO_3$, as shown in Fig. 4a–d. When 5 M $NaNO_3$ was added, the HRTEM image in Fig. 4e revealed that quasi-spherical CeO_2 particles of ~8 nm were closely attached to CNTs and were highly crystallized. When $(NH_4)_2Ce(NO_3)_6$ was used as the cerium source, the NPs attached to CNTs seemed sparser, and the size of CeO_2 NPs also decreased when $NaNO_3$ was added (Fig. 4f). XRD analysis indicated that the composites obtained at the $NaNO_3$-assisted hydrothermal conditions still obtained cubic fluorite ceria (Fig. 2). The grain size calculated by the Scherrer equation was 8.3 nm, close to 7.6 nm for CeO_2 NPs formed in absence of CNTs.

The influence of $NaNO_3$ can be understood by considering the adsorption of NO_3^- groups on the surfaces of CeO_2 nuclei. When the concentration of NO_3^- is low in a basic solution, the OH^- ions are the predominate absorbates on the surfaces of nuclei [28] and the influence of NO_3^- can be neglected. However, as the concentration of NO_3^- is increased, a large number of NO_3^- anions are adsorbed on the surfaces of nuclei and replace OH^- anions to coordinate with cerium atoms. The NO_3^- on surface could be decomposed and form surface peroxide [29]. And Sholes et al. [30] recently have found that the presence of η^2–O_2^{2-} species could decrease the CeO_2 crystallite size when H_2O_2 concentration was increased. They suggested that the O_2^{2-} coordinated to Ce(IV) play a key role in preventing the formation of a more extended crystalline CeO_2 network. In our case, the surface peroxide groups resulted from the absorbed NO_3^- might play a similar role [30].

3.3. Electrochemical performance

We examined electrochemical charge/discharge cycles of the composites prepared using $CeCl_3$ as the cerium source. These composites contained higher loading of CeO_2 NPs on CNTs than the composites prepared with $(NH_4)_2Ce(NO_3)_6$ as the cerium source. Fig. 5 showed the discharge and charge curves, and Table 1 listed the corresponding data. The composite of larger CeO_2 NPs/CNT obtained without $NaNO_3$ was denoted as CeO_2(L)/CNT, and the composite of small-sized CeO_2 particles and CNTs obtained in the presence of 5 M $NaNO_3$ was denoted as CeO_2(S)/CNT. The CNTs had the largest capacity of 700 mA h g^{-1}, while the pure CeO_2 NPs

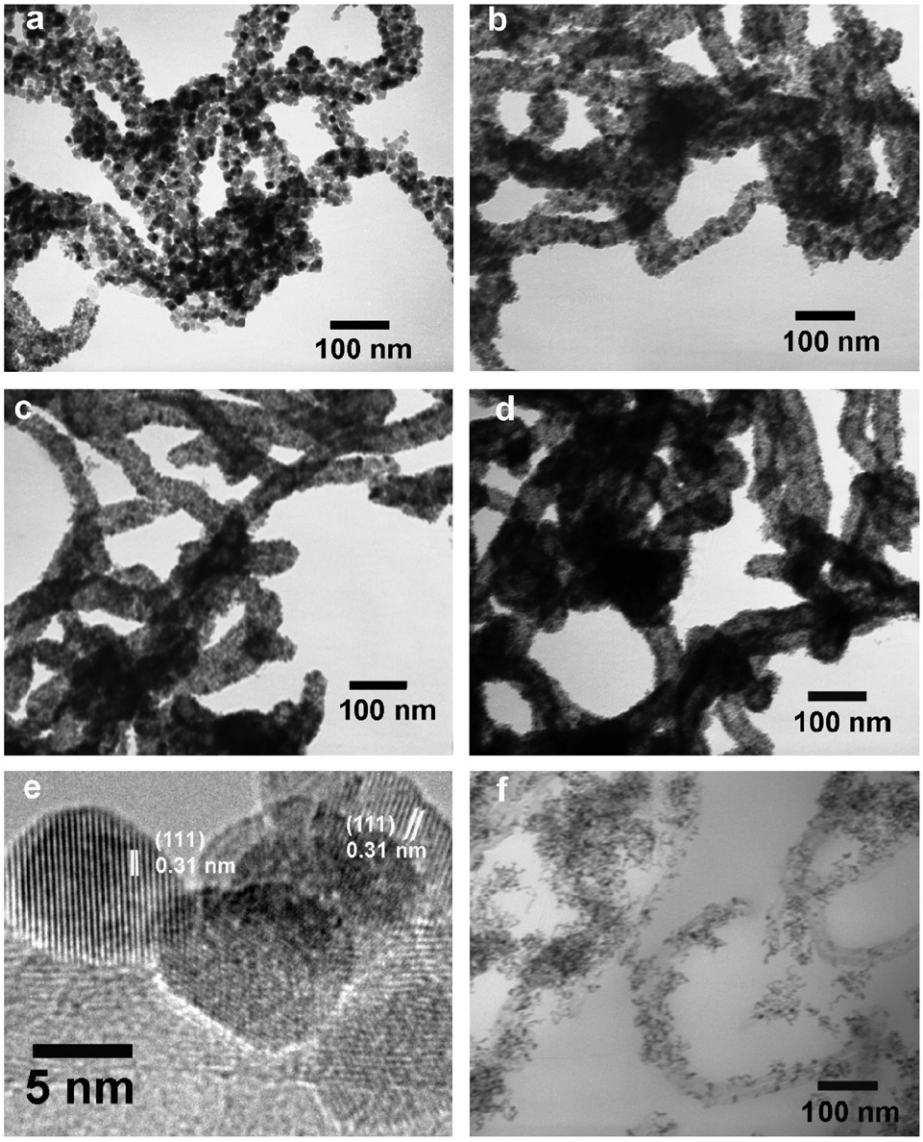

Fig. 4. TEM images of CeO_2/CNT composites prepared with $CeCl_3$ as the cerium source under different concentrations of $NaNO_3$: (a) 0.1 M, (b) 1 M, (c)3 M, (d) 5 M, (e) HRTEM image corresponding to (d), (f) TEM images of CeO_2/CNT composites hydrothermally prepared with 5 M $NaNO_3$ and $(NH_4)_2Ce(NO_3)_6$ as the cerium source.

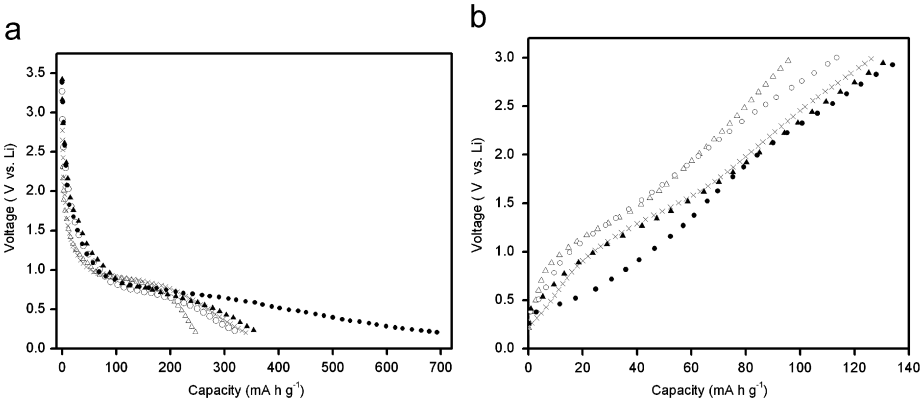

Fig. 5. Initial discharge (a) and charge (b) curves of CNTs (solid circles), CeO_2(S)/CNT composite (solid triangles), CeO_2(L)/CNT composite (cross), mechanical mixture of CeO_2 and CNTs (open circles), and CeO_2 NPs (open triangles).

had the lowest capacity of 247 mA h g^{-1}. For CeO_2/CNT composites and mechanical mixture of CeO_2 with CNTs, the capacities were from 327 to 364 mA h g^{-1}, which were between the values of CNTs and CeO_2 NPs. In addition, it appears that the CeO_2(S)/CNT composite has higher capacity. The improvement in the capacity of the CeO_2/CNT composites can be attributed to the enhanced

Table 1
Data on electrochemical performance of various active materials

	CeO_2 NPs	CeO_2(L)/CNT composite	CeO_2(S)/CNT composite	Mixture of CeO_2 and CNT	CNTs
Discharge ($mA\,h\,g^{-1}$)	247.2	339.5	363.6	327.0	700.2
Charge ($mA\,h\,g^{-1}$)	96.7	126.7	133.1	113.4	138.6
Efficiency (%)	39.1	37.3	36.6	34.7	19.8

conductivity of the samples owing to the presence of CNTs. The NPs in the composites were closely connected by the highly conductive CNTs, which acts as pathways for long-range electron transfer. Therefore, the composites possess higher electrical conductivity than either pure CeO_2 NPs or the mechanical mixture of CeO_2 NPs and CNTs [31,32]. For the CeO_2(L)/CNT composite, although its electron conductivity was improved, the Li insertion was hindered by the limited diffusion due to the larger size of the NPs [33].

Similar trend was also observed in the charging process. For anode materials of Li-ion batteries, the initial charge capacity (reversible capacity) is more important than the initial discharge capacity, because the latter might include larger irreversible capacity loss due to side reactions and formation of interphase membrane [34]. The initial coulombic efficiency, which refers to the ratio of charge capacity to discharge capacity during the first cycle, is also a very important parameter to evaluate the electrode performance. The reversible capacities for CeO_2(S)/CNT and CeO_2(L)/CNT were 133.1 and 126.7 $mA\,h\,g^{-1}$, respectively, which are both lower than that of CNTs under the same condition (138.6 $mA\,h\,g^{-1}$). However, efficiencies of the CeO_2(S)/CNT (36.6%) and CeO_2(L)/CNT (37.3%) are both higher than that of CNTs (19.8%), suggesting that more capacities in the CeO_2/CNT composites can be used than that of the CNTs during the charge/discharge cycles. So the CeO_2/CNT composites may serve as better materials for Li-ion batteries.

4. Conclusions

CeO_2 NPs/CNT composites were prepared by the hydrothermal treatment of $Ce(OH)_4$/CNT precursors at a moderate temperature of 180 °C. Due to the redox reaction between the CeO_2 nuclei and CNTs under the hydrothermal conditions, the size of the CeO_2 NPs in the composites was increased compared with those obtained without CNTs. The mechanism of the size increase was further verified by the cyclic voltammetry measurements. Addition of $NaNO_3$ can reduce the size of CeO_2 NPs. The test of charge/discharge cycle showed that the CeO_2/CNT composites have higher capacity than the mechanically mixed CeO_2 NPs and CNTs while their coulomnic efficiency is higher than that of CNTs.

Acknowledgments

The authors would like to acknowledge the financial support from NSF (projects 90406018 and 50772002), MOST (projects 2006CB932403, 2007CB936202, and 2006CB932701) of the People's Republic of China.

Appendix A. Supplementary data

Supplementary data associated with this article can be found in the online version at doi:10.1016/j.jssc.2008.06.040

References

[1] J.P. Tessonnier, L. Pesant, G. Ehret, M.J. Ledoux, C.P. Huu, Appl. Catal. A 288 (2005) 203–210.
[2] J.M. Planeix, N. Coustel, B. Coq, V. Brotons, P.S. Kumbhar, R. Dutartre, P. Geneste, P. Bernier, P.M. Ajayan, J. Am. Chem. Soc. 116 (1994) 7935–7936.
[3] Y.J. Lu, J. Li, J. Han, H.T. Ng, C. Binder, C. Partridge, M. Meyyappan, Chem. Phys. Lett. 391 (2004) 344–348.
[4] A. Star, V. Joshi, S. Skarupo, D. Thomas, J.C.P. Gabriel, J. Phys. Chem. B 110 (2006) 21014–21020.
[5] Y.T. Kim, K. Tadai, T. Mitani, J. Mater. Chem. 15 (2005) 4914–4921.
[6] J. Prabhuram, T.S. Zhao, Z.K. Tang, R. Chen, Z.X. Liang, J. Phys. Chem. B 110 (2006) 5245–5252.
[7] D.M. Guldi, G.M.A. Rahman, V. Sgobba, N.A. Kotov, D. Bonifazi, M. Prato, J. Am. Chem. Soc. 128 (2006) 2315–2323.
[8] J.M. Haremza, M.A. Hahn, T.D. Krauss, Nano Letters 2 (2002) 1253–1258.
[9] I. Robel, B.A. Bunker, P.V. Kamat, Adv. Mater. 17 (2005) 2458–2463.
[10] A. Trovarelli, C. Leitenburg, M. Boaro, G. Dolcetti, Catal. Today 50 (1999) 353–367.
[11] S. Park, J.M. Vohs, R.J. Gorte, Nature 404 (2000) 265–267.
[12] T. Morimoto, H. Tomonaga, A. Mitani, Thin Solid Films 35 (1999) 61–65.
[13] P. Dutta, S. Pal, M.S. Seehra, Chem. Mater. 18 (2006) 5144–5146.
[14] Y.H. Li, J. Ding, J.F. Chen, C.L. Xu, B.Q. Wei, J. Liang, D.H. Wu, Mater. Res. Bull. 37 (2002) 313–318.
[15] J.Q. Wei, J. Ding, X.F. Zhang, D.H. Wu, Z.C. Wang, J.B. Luo, K.L. Wang, Mater. Lett. 59 (2005) 322–325.
[16] X.J. Peng, Z.K. Luan, J. Ding, Z.C. Di, Y.H. Li, B.H. Tian, Mater. Lett. 59 (2005) 399–403.
[17] Z.C. Di, J. Ding, X.J. Peng, Y.H. Li, Z.K. Luan, J. Liang, Chemsphere 62 (2006) 861–865.
[18] D. Zhao, E. Han, X. Wu, H. Guan, Mater. Lett. 60 (2006) 3544–3547.
[19] D.S. Zhang, L.Y. Shi, H.X. Fu, J.H. Fang, Carbon 44 (2006) 2853–2855.
[20] R.Q. Yu, L.W. Chen, Q.P. Liu, J.Y. Lin, K.L. Tan, S.C. Ng, H.S.O. Chan, G.Q. Xu, T.A. Hor, Chem. Mater. 10 (1998) 718–722.
[21] N.C. Wu, E.W. Shi, Y.Q. Zheng, W.J. Li, J. Am. Ceram. Soc. 85 (2002) 2462–2468.
[22] H.X. Mai, L.D. Sun, Y.W. Zhang, R. Si, W. Feng, H.P. Zhang, C.H. Yan, H.C. Liu, J. Phys. Chem. B 109 (2005) 24380–24385.
[23] D.S. Zhang, L.Y. Shi, J.H. Fang, Q. Li, J. Solid State Chem. 180 (2007) 654–660.
[24] M. Nolan, S.C. Parker, G.W. Watson, J. Phys. Chem. B 110 (2006) 2256–2262.
[25] A.B. López, K. Krishna, M. Makkee, J.A. Moulijn, Catal. Lett. 99 (2005) 203–205.
[26] Z.H. Kang, E.B. Wang, B.D. Mao, Z.M. Su, L. Gao, L. Niu, H.Y. Shan, L. Xu, Appl. Catal. A 299 (2006) 212–217.
[27] J.H. Chen, M.Y. Wang, Bo Liu, Z. Fan, K.Z. Cui, Y.F. Kuang, J. Phys. Chem. B 110 (2006) 11775–11779.
[28] R. Si, Y.W. Zhang, L.P. You, C.H. Yan, J. Phys. Chem. B 110 (2006) 5994–6000.
[29] A. Setiabudi, J.L. Chen, G. Mul, M. Makkee, J.A. Moulijn, Appl. Catal. B: Environ. 51 (2004) 9–19.
[30] F.H. Scholes, A.E. Hughes, S.G. Hardin, P. Lynch, P.R. Miller, Chem. Mater. 19 (2007) 2321–2328.
[31] I.V. Thorat, V. Mathur, J.N. Harb, D.R. Wheeler, J. Power Source 162 (2006) 673–678.
[32] X.L. Li, F.Y. Kang, X.D. Bai, W.C. Shen, Electrochem. Commun. 9 (2007) 663–666.
[33] J.M. Tarascon, C. Delacourt, A.S. Prakash, M. Morcrette, M.S. Hegde, C. Wurm, C. Masquelier, Dalton Trans. (2004) 2988–2994.
[34] F.S. Ke, L. Huang, J.S. Cai, S.G. Sun, Electrochim. Acta 52 (2007) 6741–6747.